Mechanisms of Podocyte Injury in Diabetes
Role of Cytochrome P450 and NADPH Oxidases

Assaad A. Eid,[1] Yves Gorin,[1] Bridget M. Fagg,[1] Rita Maalouf,[1] Jeffrey L. Barnes,[1,2] Karen Block,[1,2] and Hanna E. Abboud[1,2]

OBJECTIVE—We investigated the role of cytochrome P450 of the 4A family (CYP4A), its metabolites, and NADPH oxidases both in reactive oxygen species (ROS) production and apoptosis of podocytes exposed to high glucose and in OVE26 mice, a model of type 1 diabetes.

RESEARCH DESIGN AND METHODS—Apoptosis, albuminuria, ROS generation, NADPH superoxide generation, CYP4A and Nox protein expression, and mRNA levels were measured in vitro and in vivo.

RESULTS—Exposure of mouse podocytes to high glucose resulted in apoptosis, with approximately one-third of the cells being apoptotic by 72 h. High-glucose treatment increased ROS generation and was associated with sequential upregulation of CYP4A and an increase in 20-hydroxyeicosatetraenoic acid (20-HETE) and Nox oxidases. This is consistent with the observation of delayed induction of NADPH oxidase activity by high glucose. The effects of high glucose on NADPH oxidase activity, Nox proteins and mRNA expression, and apoptosis were blocked by *N*-hydroxy-*N*′-(4-butyl-2-methylphenol) formamidine (HET0016), an inhibitor of CYP4A, and were mimicked by 20-HETE. CYP4A and Nox oxidase expression was upregulated in glomeruli of type 1 diabetic OVE26 mice. Treatment of OVE26 mice with HET0016 decreased NADPH oxidase activity and Nox1 and Nox4 protein expression and ameliorated apoptosis and albuminuria.

CONCLUSIONS—Generation of ROS by CYP4A monooxygenases, 20-HETE, and Nox oxidases is involved in podocyte apoptosis in vitro and in vivo. Inhibition of selected cytochrome P450 isoforms prevented podocyte apoptosis and reduced proteinuria in diabetes. ***Diabetes*** **58:1201–1211, 2009**

Diabetic nephropathy in humans is characterized by increased urinary albumin excretion (microalbuminuria), which often progresses to proteinuria, one of the most important prognostic risk factors for kidney disease progression (1). Glomerular visceral epithelial cells, or podocytes, play a critical role in maintaining the structure and function of the glomerular filtration barrier. Careful morphometric analyses of renal biopsy in subjects with type 1 and type 2 diabetes (2–4) demonstrate that the density of podocytes is reduced not only in individuals with diabetic nephropathy, but also in patients with short duration of diabetes before the onset of microalbuminuria (4,5). Studies in experimental models of type 1 and type 2 diabetes have also documented that podocyte depletion represents one of the earliest cellular lesions affecting the diabetic kidney (6,7). Among various morphologic characteristics, the decreased number of podocytes in glomeruli is the strongest predictor of progression of diabetic nephropathy, where fewer cells predict more rapid progression (3,4). Although these observations identify podocyte depletion as one of the earliest cellular features of diabetic kidney disease, the mechanisms that underlie the loss of podocytes in diabetic nephropathy remain poorly understood.

High glucose induces apoptosis (8), and there is evidence that podocyte apoptosis contributes to reduced podocyte number (9). High glucose, transforming growth factor-β (TGF-β), and angiotensin II (ANGII) induce apoptosis of cultured podocytes (9–12). ANGII appears to induce apoptosis in cultured rat glomerular epithelial cells at least partially via TGF-β because its apoptotic effect is attenuated by an anti–TGF-β antibody (12). There is also evidence that reactive oxygen species (ROS) contribute to podocyte apoptosis and depletion in cells exposed to high glucose and in experimental diabetic nephropathy (7). However, the sources of ROS and the kinetics of their generation have not been well characterized. We and others (13–15) have recently identified NADPH oxidases as major sources of ROS in kidney cortex and glomeruli of rats with type 1 diabetes. Six homologs of the cytochrome subunit of the phagocyte NADPH oxidase (Nox2/gp91^{phox}) have been cloned (16). At least three different Nox isoforms are expressed in the kidney cortex: Nox1, Nox2, and Nox4 (16). Cytochromes P450 (CYP450s) are significant sources of ROS in many tissues (17,18). CYP450 metabolizes arachidonic acid into hydroxyeicosatetraenoic acids (20-HETEs) and EETs (epoxyeicosatrienoic acids). 20-HETE, the ω-hydroxylation product of arachidonic acid, is one of the major CYP eicosanoids produced in the kidney cortex (19–21). The predominant CYP450 in the kidney cortex that synthesizes 20-HETE is cytochrome P450 of the 4A family (CYP4A) (19–21). 20-HETE has multiple and opposing functions depending on the site of production and target cells/tissues (19,22–24).

In this study, we demonstrate that high glucose induces ROS production and apoptosis in cultured mouse podocytes through the upregulation of CYP4A with increased production of 20-HETE and upregulation of NADPH oxidases. Inhibition of 20-HETE production prevented podocyte apoptosis in vitro and decreased oxidative stress, podocyte apoptosis, and proteinuria in an in vivo model of type 1 diabetes.

From the [1]University of Texas Health Science Center, Department of Medicine, San Antonio, Texas; and the [2]South Texas Veterans Healthcare System, San Antonio, Texas.
Corresponding author: Hanna E. Abboud, abboud@uthscsa.edu.
Received 4 November 2008 and accepted 5 February 2009.
Published ahead of print at http://diabetes.diabetesjournals.org on 10 February 2009. DOI: 10.2337/db08-1536.

RESEARCH DESIGN AND METHODS

Conditionally immortalized mouse podocytes, kindly provided by Dr. Peter Mundel (University of Florida, Miami, Florida), were cultured as previously described (20,25). In brief, cells were first grown under permissive conditions at 33°C in RPMI-1640 media containing 10% FCS, 50 units/ml interferon(IFN)-γ (IFN), and 100 units/ml of penicillin/streptomycin in collagen-coated flasks. Concentration of IFN-γ was then tapered to 10 units/ml, and cells were subcultivated under nonpermissive conditions (37°C) in serum-containing medium without IFN-γ. Near-confluent cells were growth-arrested in RPMI-1640 containing 0.2% BSA (fatty-acid free) and 5 mmol/l D-glucose for 24 h before the experiment.

Animal models. We used 7-month-old FVB and OVE26 mice on FVB background (Jackson Laboratories, Bar Harbor, ME). At 6 months of age, OVE26 mice were treated with *N*-hydroxy-*N*′-(4-butyl-2-methylphenol) formamidine (HET0016), a specific inhibitor of CYP4A, for 3 weeks. Mice were placed in metabolic cages for urine collection, and before the treatment with HET0016, urine albumin was measured by an Albuwell M test kit (Exocell, Philadelphia, PA) and expressed as micrograms of albumin per 24 h. Animals were killed by exsanguination under anesthesia. Both kidneys were removed and weighed. A slice of kidney cortex at the pole was embedded in paraffin or flash-frozen in liquid nitrogen for microscopy and image analyses. Cortical tissue was used for isolation of glomeruli by differential sieving with minor modification as previously described (26).

Detection of intracellular ROS. The peroxide-sensitive fluorescent probe 2′,7′-dichlorodihydrofluorescin (DCF) diacetate (Molecular Probes) was used to measure intracellular ROS as previously described (15). Cells were grown in 12- or 24-well plates and serum-deprived for 24 h. Immediately before the experiments, cells were washed with Hank's buffered salt solution containing Ca^{2+} and Mg^{2+} and then loaded with 50 μmol/l DCF diacetate dissolved in Hank's buffered salt solution for 30 min at 37°C. Cells were then incubated for 45 min with HET0016 followed by the addition of the agonist or vehicle for various time periods. DCF fluorescence was detected at excitation and emission wavelengths of 488 and 520 nm, respectively, and measured in a multiwell fluorescence plate reader (Wallac 1420 Victor^2; PerkinElmer).

NADPH oxidase activity. NADPH oxidase activity was measured in podocytes grown in serum-free medium or in glomeruli isolated from kidney cortex as previously described (13). Cultured podocytes were washed five times in ice-cold PBS and scraped from the plate in the same solution followed by centrifugation at 800 rpm, 4°C, for 10 min. The cell pellets were resuspended in lysis buffer (20 mmol/l KH_2PO_4, pH 7.0, 1 mmol/l EGTA, 1 mmol/l phenylmethylsulfonyl fluoride (PMSF), 10 μg/ml aprotinin, and 0.5 μg/ml leupeptin). Cell suspensions or washed glomeruli were homogenized with 100 strokes in a Dounce homogenizer on ice. To start the assay, 20 μg of homogenates were added to 50 mmol/l phosphate buffer, pH 7.0, containing 1 mmol/l EGTA, 150 mmol/l sucrose, 5 μmol/l lucigenin, and 100 μmol/l NADPH. Photon emission expressed as relative light units was measured every 20 or 30 s for 10 min in a luminometer. A buffer blank (<5% of the cell signal) was subtracted from each reading. Superoxide production was expressed as relative light units per milligrams of protein. Protein content was measured using a Bio-Rad protein assay reagent.

Isolation of microsomes. Podocytes in serum-free medium or glomeruli isolated from kidney cortex were homogenized in a 10 mmol/l potassium phosphate buffer, pH 7.7, containing 250 mmol/l sucrose, 1 mmol/l EDTA, 10 mmol/l magnesium chloride, 2 μmol/l leupeptin, 1 μmol/l pepstatin, 2 μg/ml aprotinin, and 0.1 μmol/l PMSF. Microsomes were prepared by differential centrifugation as previously described (27,28) and used for Western blotting and 20-HETE measurement by high-performance liquid chromatography (HPLC).

Western blotting analysis. Homogenates from glomeruli isolated from renal cortex were prepared in 200 μl of radioimmune precipitation assay buffer (20 mmol/l Tris·HCl, pH 7.5, 150 mmol/l NaCl, 5 mmol/l EDTA, 1 mmol/l Na_3VO_4, 1 mmol/l PMSF, 20 μg/ml aprotinin, 20 μg/ml leupeptin, and 1% NP-40) using a Dounce homogenizer. Homogenates were incubated for 1 h at 4°C and centrifuged at 10,000 rpm for 30 min at 4°C.

Mice podocytes were grown to near confluency in 60- or 100-mm dishes and serum deprived for 24 h. All incubations were carried out in serum-free RPMI containing 0.2% BSA (fatty acid free) at 37°C for a specified duration. The cells were lysed in radioimmune precipitation buffer at 4°C for 30 min. The cell lysates were centrifuged at 10,000 rpm for 30 min at 4°C. Protein in the supernatants was measured using the Bio-Rad method. For immunoblotting, proteins (40–80 μg) were separated on 12.5% SDS-PAGE and transferred to polyvinylidene difluoride membranes. Blots were incubated with rabbit polyclonal anti-Nox1 (1:200 H-75; Santa Cruz Biotechnology), rabbit polyclonal anti-Nox2 (1:1,000; Upstate), rabbit polyclonal anti-Nox4 (1:1,000; Novus Biological), and rabbit polyclonal anti-CYP4A (1:500, Abcam). The primary antibodies were detected using horseradish peroxidase–conjugated IgG (1:2,500 or 1:5,000). Bands were visualized by enhanced chemiluminescence. Densitometric analysis was performed using National Institutes of Health Image software.

20-HETE production. Levels of 20-HETE were measured in isolated microsomes by HPLC. In short, [1-^{14}C]-labeled arachidonic acid (50–100 μmol/l) was dried down and resuspended in the reaction mix containing 50 μg microsomes, 30 mmol/l isocitrate, and 0.2 unit isocitrate dehydrogenase in reaction buffer (100 mmol/l potassium phosphate, pH 7.4, 5 mmol/l magnesium chloride, and 1 mmol/l EDTA). After incubation at 37°C for 5 min, the reaction was initiated by the addition of NADPH to a final concentration of 1 mmol/l. Aliquots were removed at 30, 60, and 90 min, and the reaction was stopped by the addition of 100% methanol. The precipitated proteins were then pelleted by centrifugation (in a microcentrifuge), and the samples were stored at −20°C until analyzed. The metabolites were separated via HPLC on a C-18 column using an acetonitrile/H20 gradient and identified by coelution with labeled standards.

mRNA analysis. mRNA was analyzed by real-time RT-PCR using the $\Delta\Delta C_t$ method. Total RNA was isolated from cultured mouse podocytes using an RNeasy Mini kit from Qiagen. mRNA expression was quantified using a Realplex mastercycler (Eppendorf, Westbury, NY) with SYBR green dye and mouse RT^2 qPCR Primers (SABiosciences, Frederick, MD) for Nox1 (sequence accession no. NM_172203) and Nox4 (sequence accession no. NM_015760) and normalized to GAPDH.

Hoechst staining. Cells were plated on plastic four-chamber slides. Apoptotic nuclei were detected using Hoechst 33258 (Fluka) staining (1 μg/ml, 30 min) in cells fixed with 4% paraformaldehyde and analyzed via fluorescence microscopy at 350-nm excitation and 460-nm emission.

Annexin V and propidium iodide staining. An annexin V–fluorescein isothiocyanate (FITC) apoptosis detection kit (Calbiochem) was used for annexin V and propidium iodide staining according to the manufacturer protocol. Podocytes were cultured in 60 mm dishes to ~ 80% confluency and serum-starved for 24 h. Cells were then preincubated with or without 10 μmol/l HET0016 before the addition of glucose (25 mmol/l) or 1 μmol/l of 20-HETE. Cells were then incubated for 24, 48, or 72 h at 37°C. The percentage of apoptotic and necrotic cells was assessed by fluorescence-activated cell sorting (San Antonio Cancer Institute core facility of the University of Texas Health Science Center San Antonio).

Electron microscopy. Kidney cortexes isolated from the FVB, OVE 26, and OVE26 mice treated with HET0016 were cut into 0.5- to 1-mm^3 pieces and fixed overnight in cold 4% formaldehyde and 1% glutaraldehyde in phosphate buffer and then embedded in epon 812 resin. Then, 0.5-mm plastic sections were cut and stained with toluidine blue for identification of representative areas for subsequent sectioning by ultramicrotome. Ultrathin sections were stained with uranyl acetate and examined and photographed on a JEOL 100CX electron microscope. All electron microscope (EM) photomicrographs were examined in a blind fashion. Individual capillary loops were examined and quantified in five glomeruli per group of animals (FVB, OVE26, and OVE 26 mice treated with HET0016) for the degree of foot process effacement as described by Jo et al. (29).

Podocyte enumeration. Dual-label immunohistochemistry was used to identify and count glomerular epithelial cells relative to the glomerular basement membrane (GBM) using a modification of methods previously described (30). To identify podocytes, 3-μm frozen sections of kidney cortex on glass slides were stained with a goat anti-synaptopodin antibody (Santa Cruz Biotechnology) followed by Cy3-labeled donkey anti-goat IgG (Chemicon). After washing, and to identify the GBM, the sections were stained with a rabbit antibody directed against collagen type IV (Chemicon) followed by FITC-labeled donkey anti-rabbit IgG (Chemicon). After staining and washing, the sections were preserved on coverslips in Prolong gold antifade mounting medium with 4′,6-diamidino-2-phenylindole (Invitrogen) for the fluorescence detection of nuclei. Sections were examined by epifluorescence using excitation and band-pass filters optimal for FITC, Cy3, and 4′,6-diamidino-2-phenylindole. Digital images representing each fluorochrome were taken of random glomeruli using an AX70 Research microscope and a DP70 digital camera (Olympus, Melville, NY). Then, 25–30 glomerular cross-sections per animal were photographed in each color channel providing a minimum of 100 composite images per experimental group. The images were merged and color balanced using Image-Pro Plus imaging software (Media Cybernetics, Silver Spring, MD), and podocytes were counted in projected images in a blind fashion by two individuals. Synaptopodin-positive cells on the outer aspect of the GBM were considered glomerular epithelial cells and counted. Synaptopodin-negative cells or those in the inner aspect of the GBM were not counted. The mean area of each glomerular profile was measured manually, tracing the glomerular outline, encircling the area of interest, and calculating the surface area by computerized morphometry using MetaMorph 4.69. The results were expressed as the average number of podocytes per glomerular section as previously described (31–33).

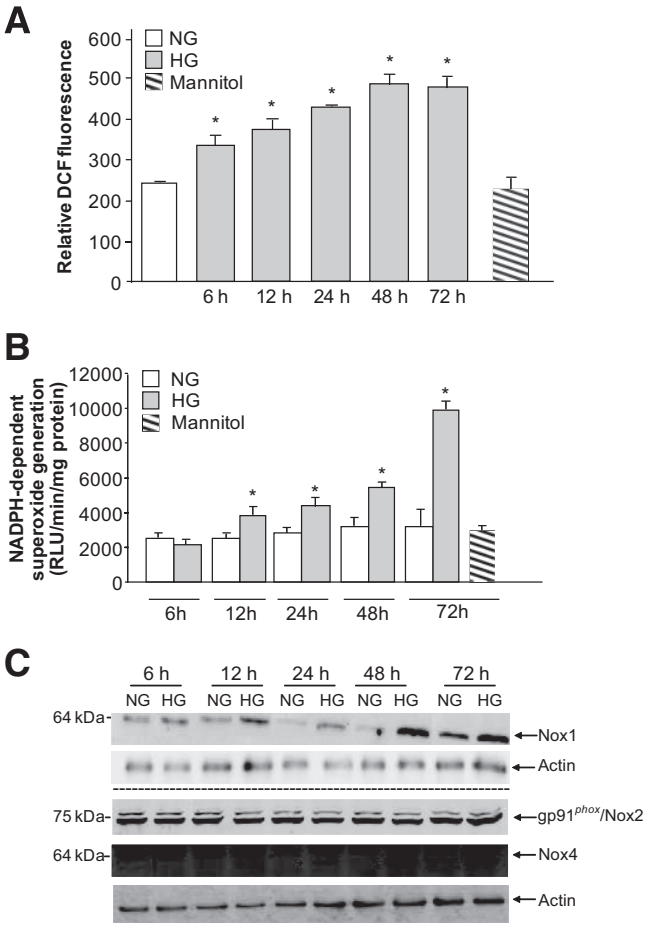

FIG. 1. Temporal effect of high glucose on ROS generation in mouse podocytes. *A*: Mouse podocytes were exposed to either high glucose (HG; 25 mmol/l) or normal glucose (NG; 5 mmol/l) for the indicated time periods. ROS generation was measured by DCF with a multiwell fluorescence plate reader as described in RESEARCH DESIGN AND METHODS. Values are the means ± SE of three independent experiments (n = 3). *P < 0.05, high glucose vs. control. *B*: Mouse podocytes were exposed to either high glucose (25 mmol/l) or normal glucose (5 mmol/l) for the indicated time periods. NADPH-dependent superoxide generation was assessed by lucigenin-enhanced chemiluminescence. Superoxide anion was expressed as relative chemiluminescent light units (RLU) per milligram of protein per minute (n = 3). *C*: Expression of Nox1, Nox2, and Nox4 protein was determined by Western blotting analysis on homogenized podocytes. Actin was included as a control for loading and the specificity of change in protein expression. The Western blot is representative of three independent experiments (n = 3).

RESULTS

High glucose induces oxidative stress in podocytes. Exposure of podocytes to 25 mmol/l glucose (high glucose) results in a relatively rapid generation of ROS, as measured by DCF fluorescence, compared with cells incubated in 5 mmol/l glucose (normal glucose) or mannitol used as an osmotic control. ROS generation was detected after 6 h of exposure to high glucose and was sustained up to 72 h (Fig. 1*A*). NADPH oxidases of the Nox family are major sources of ROS in cells and tissue (13,15,16). However, there was no increase in NADPH-dependent superoxide generation 6 h after exposure of the cells to high glucose (Fig. 1*C*). The increase in NADPH oxidase activity was detectable only at 12 h and remained sustained up to 72 h (Fig. 1*B*), suggesting that other sources of ROS besides NADPH oxidases were involved in the ROS generation seen at early time points after treatment with high glucose. Consistent with these observations, we found that upregulation of the two major Nox isoforms, Nox1 and Nox4, was not seen before 12 and 24 h, respectively. Note that Nox2 isoform expression was not altered by high-glucose treatment.

High glucose induces CYP4A protein expression and 20-HETE production. We next examined whether CYP4A contributes to oxidative stress induced by high glucose in mouse podocytes. Microsomes were isolated from podocytes incubated in normal or high glucose. Our data show that CYP4A protein expression was increased in microsomes isolated from podocytes incubated in the presence of high glucose compared with podocytes incubated in normal glucose, with maximum expression seen at 6 and 12 h (Fig. 2*A*). The increase of CYP4A protein expression was accompanied by an increase in 20-HETE formation, the major biologically active metabolite produced by CYP4A (Fig. 2*B*).

20-HETE generated by CYP4A mediates the effect of high glucose on ROS generation. We next determined whether CYP4A-derived 20-HETE mediates the effect of high glucose on ROS generation in podocytes. DCF fluorescence was used to measure ROS in mouse podocytes exposed to high glucose, in the absence or presence of *N*-hydroxy-*N*′-(4-butyl-2-methylphenol) formamidine (HET0016; 10 μmol/l, 1 h), a potent inhibitor of CYP4A (20-HETE biosynthesis) (34). The increase in ROS generation induced by high glucose was inhibited by HET0016 (Fig. 2*C*). Moreover, we show that purified recombinant 20-HETE (1 μmol/l) mimicked the effect of high glucose on ROS production in podocytes (Fig. 2*C*). Collectively, these data indicate that 20-HETE, the major product of the CYP4A pathway, mediated the effect of high glucose on ROS in podocytes. Furthermore, the data indicate that the increase in ROS in podocytes was likely caused by sequential activation of CYP4A and activation of Nox oxidases.

Redox pathway implicating CYP4A-dependent generation of 20-HETE mediates the effect of high glucose on podocyte apoptosis. High glucose has been shown to induce podocyte apoptosis (7). Data in Fig. 3*A* and *B* show that high glucose induced podocyte apoptosis, as assessed by annexin V binding and Hoechst staining. This effect was blocked by the pretreatment of the cells with HET0016, suggesting that CYP4A contributed to the apoptotic effect of glucose in podocytes. This concept was further supported by the finding that 20-HETE mimicked the effect of glucose and induced podocyte apoptosis (Fig. 3*A* and *B*). These findings indicate that the increased CYP4A/20-HETE production induced ROS generation and resulted in podocyte apoptosis. Annexin V–binding assay detects the translocation of phosphatidylserine to the cell surface, an early event in cells undergoing apoptosis. Hoechst staining, on the other hand, shows the number of cells with chromatin condensation, i.e., that have already undergone apoptosis.

20-HETE generation by CYP4A mediates the effect of high glucose on NADPH oxidase activity and Nox protein expression and mRNA levels. The observation that upregulation of CYP4A expression preceded that of Nox1 and Nox4 oxidases suggests that CYP4A and its product 20-HETE are responsible for the increased expression of Nox oxidases and contribute to high-glucose–induced oxidative stress in podocytes. Nox1 and Nox4 protein and mRNA levels were measured in mouse podocytes exposed to high glucose in the absence or presence of 10 μmol/l HET0016. High glucose increased the expression of Nox1 and Nox4 proteins as well as mRNA levels of both oxidases. The increase in Nox1 and Nox4 protein and

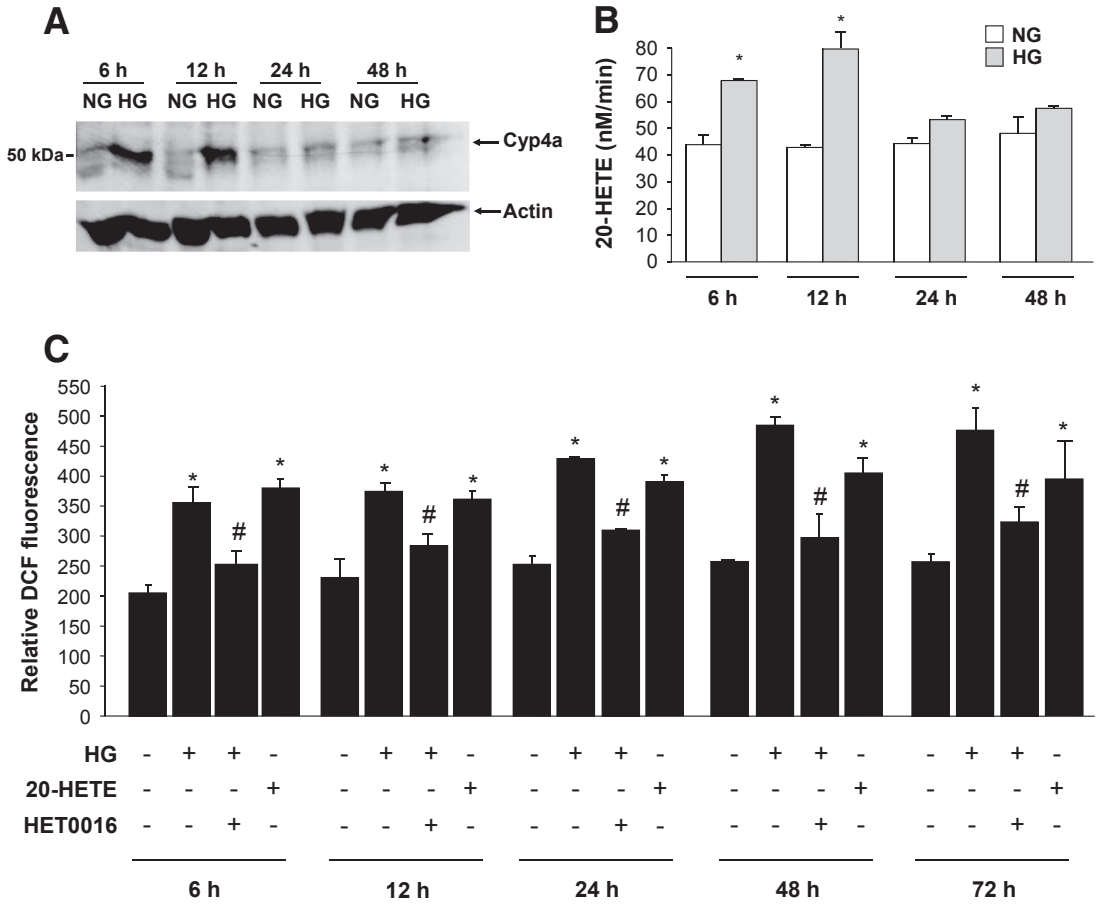

FIG. 2. CYP4A-dependent 20-HETE production mediates high-glucose–induced ROS generation in mouse podocytes. Serum-deprived podocytes were preincubated with or without HET0016 (10 μmol/l) for 1 h and treated with high glucose (HG; 25 mmol/l) or with 1 μmol/l of pure recombinant 20-HETE for the indicated time periods. *A*: Expression of CYP4A protein was determined by Western blotting analysis on microsomes isolated from mouse podocytes. The Western blot is representative of three independent experiments ($n = 3$). *B*: Microsomes (0.25 mg of protein) prepared from podocytes were incubated with 10 μmol/l arachidonic acid in the presence of NADPH. 20-HETE was separated by reverse-phase HPLC. Values of three independent experiments ($n = 3$) are the means ± SE. *$P < 0.05$, high glucose vs. normal glucose. *C*: DCF fluorescence was measured as in Fig. 1. Values are the means ± SE of three independent experiments ($n = 3$). *$P < 0.05$, high glucose or 20-HETE vs. normal glucose; #$P < 0.05$, high glucose vs. high glucose + HET0016.

mRNA levels in cells exposed to high glucose was inhibited by pretreatment of the cells with HET0016 (Fig. 4*A–C*). Moreover, treatment of the cells with 1 μmol/l 20-HETE mimicked the effect of high glucose and resulted in an increase in mRNA levels and protein expression of Nox1 and Nox4 (Fig. 4*A–C*). These effects were paralleled by changes in NADPH oxidase activity (Fig. 4*D*).

CYP4A and 20-HETE mediate diabetes-induced podocyte apoptosis in OVE26 mice. To determine the in vivo relevance of the findings in cultured cells, OVE26 mice were treated with HET0016 for 3 weeks. Mice were killed, and findings were compared with nontreated OVE 26 mice and their FVB littermates. The protein expression of CYP4A was increased in microsomes isolated from glomeruli of OVE26 mice compared with control FVB mice (Fig. 5*A*). NADPH oxidase activity and Nox1/Nox4 protein expression were upregulated in the OVE26 mice and were significantly decreased in OVE26 mice treated with HET0016 (Fig. 5*B* and *C*). Treatment with HET0016 also resulted in a decrease in foot process effacement, podocyte apoptosis as observed by EM (Fig. 6*A* and *B*), and synaptopodyn protein expression as assessed by immunohistochemistry (Fig. 7*A–C*). OVE26 diabetic mice treated with HET0016 exhibited a significant decrease in albumin excretion. Values for urine protein are as follows: 0.035 ± 0.009 mg per 24 h for the FVB control mice, 4.55 ± 0.6 mg per 24 h for the OVE26 diabetic mice, and 2.37 ± 0.9 mg per 24 h for the OVE26 diabetic mice treated with HET0016 (Fig. 8). Altogether, these data show that ROS generation through CYP4A and Nox oxidases plays a critical role in podocyte injury and albuminuria in type 1 diabetes.

DISCUSSION

Podocyte apoptosis is an early glomerular phenotype that contributes to progressive podocyte depletion and albuminuria (7). Oxidative stress has been implicated in the pathogenesis of diabetes complications, including podocyte apoptosis (13,15,35). We demonstrate that high glucose induces apoptosis of cultured podocytes through the generation of ROS via sequential upregulation of CYP4A and the NADPH oxidases Nox1 and Nox4. We demonstrate, for the first time, that 20-HETE, the major product of CYP4A, enhanced NADPH-dependent superoxide anion generation, upregulated the expression of Nox1 and Nox4 proteins, and induced podocyte apoptosis. Inhibition of CYP4A prevented oxidative stress and podocyte apoptosis in vitro and reduced

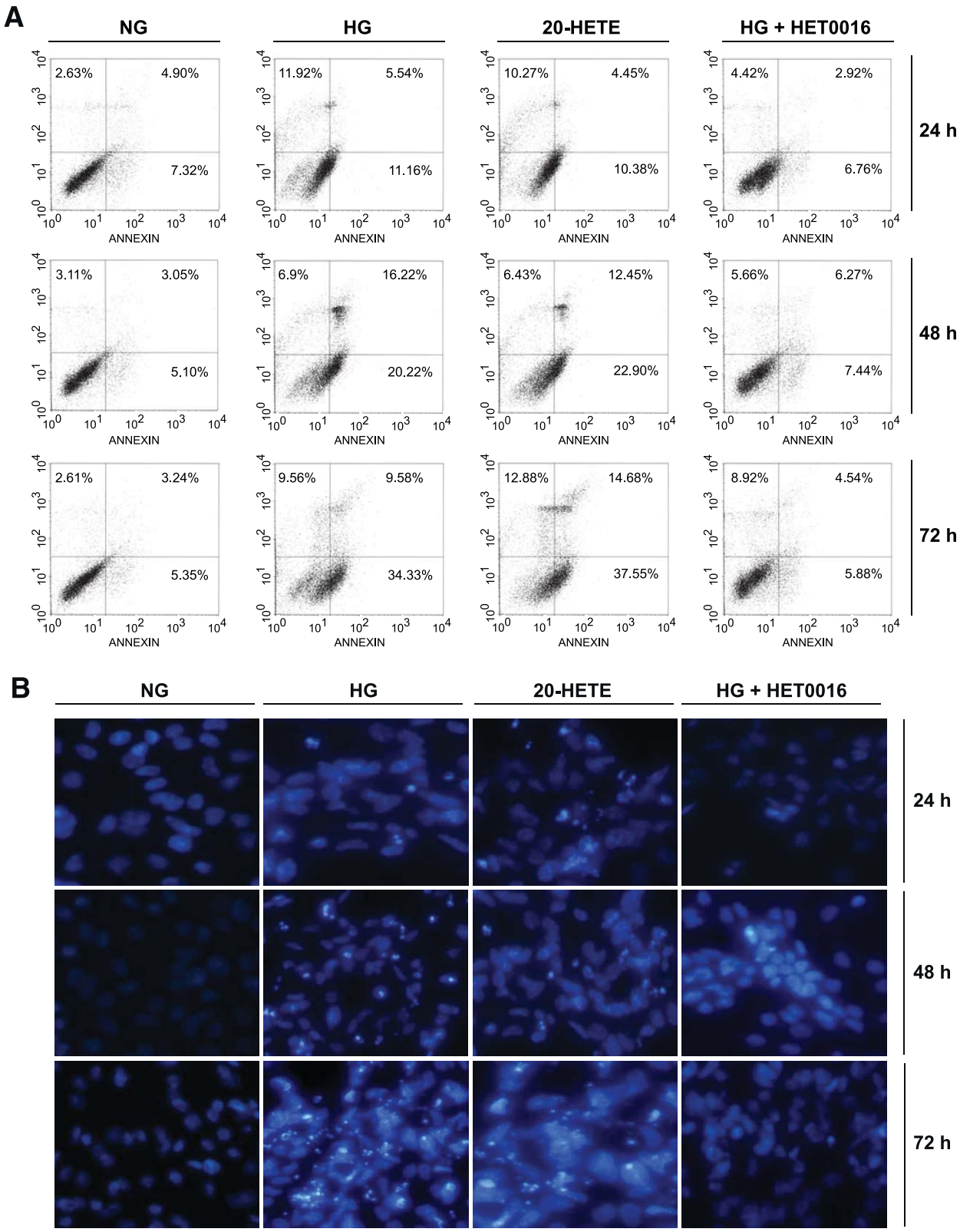

FIG. 3. CYP4A-dependent 20-HETE production mediates high-glucose–induced podocyte apoptosis. Serum-deprived podocytes were preincubated with or without HET0016 (10 μmol/l) for 1 h and then treated with high glucose (HG; 25 mmol/l), normal glucose (NG; 5 mmol/l), or 1 μmol/l of recombinant 20-HETE for the indicated time periods. *A*: Representative photographs of annexin V and propidium iodide staining in different groups (n = 3 in each group). The number of apoptotic or necrotic cells was quantified by FACS analysis after staining with annexin V and propidium iodide. The cytograms show viable cells that did not bind annexin V or propidium iodide in the left lower quadrant. Cells at early stages of apoptosis that bound annexin V but that still had intact cell membranes and excluded propidium iodide are shown in the lower right quadrant. Cells with advanced stages of apoptosis or necrotic cells were both annexin V positive and propidium iodide positive and are shown in the upper right quadrant. *B*: Apoptotic nuclei were detected using Hoechst 33258. Chromatin condensation was examined by fluorescent microscopy. (A high-quality digital representation of this figure can be found in the online issue.)

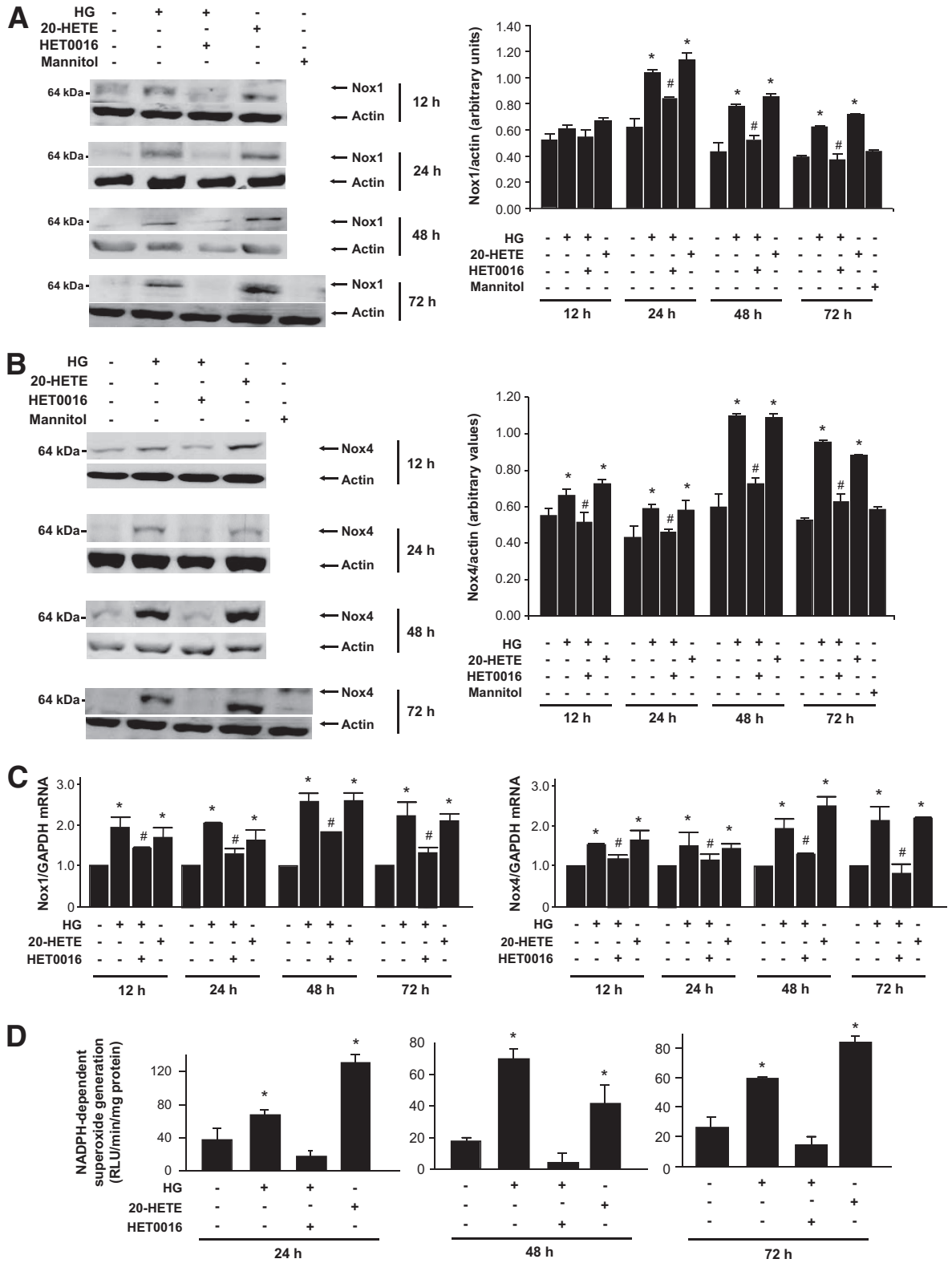

FIG. 4. CYP4A-dependent 20-HETE production mediates high-glucose–induced Nox1 and Nox4 protein expression and NADPH oxidase activation. Serum-deprived podocytes were preincubated with or without HET0016 (10 μmol/l) for 1 h and treated with high glucose (HG; 25 mmol/l), normal glucose (NG; 5 mmol/l), or 1 μmol/l of pure recombinant 20-HETE for the indicated time periods. Expression of Nox1 (*A*) and Nox4 (*B*) protein was determined by Western blotting analysis on homogenized podocytes. The Western blots are representative of three independent experiments ($n = 3$). Each histogram represents the ratio of the intensity of the Nox1 or Nox4 bands factored by the actin band. Values are the means ± SE. *$P < 0.05$, high glucose or 20-HETE vs. normal glucose; #$P < 0.05$, high glucose vs. high glucose + HET0016. *C*: Nox1 and Nox4 mRNA levels. The values represent the relative induction as measured by real-time RT-PCR relative to GAPDH mRNA levels ($n = 3$). The values are the means ± SE. *$P < 0.05$, high glucose or 20-HETE vs. normal glucose; #$P < 0.05$, high glucose vs. high glucose + HET0016. *D*: NADPH-dependent ROS generation in podocyte homogenates was measured by lucigenin-enhanced chemiluminescence. Superoxide anion is expressed as relative chemiluminescent light units (RLU) per milligram of protein per minute. Values of three independent experiments ($n = 3$) are the means ± SE. *$P < 0.05$, high glucose or 20-HETE vs. normal glucose; #$P < 0.05$, high glucose vs. high glucose + HET0016.

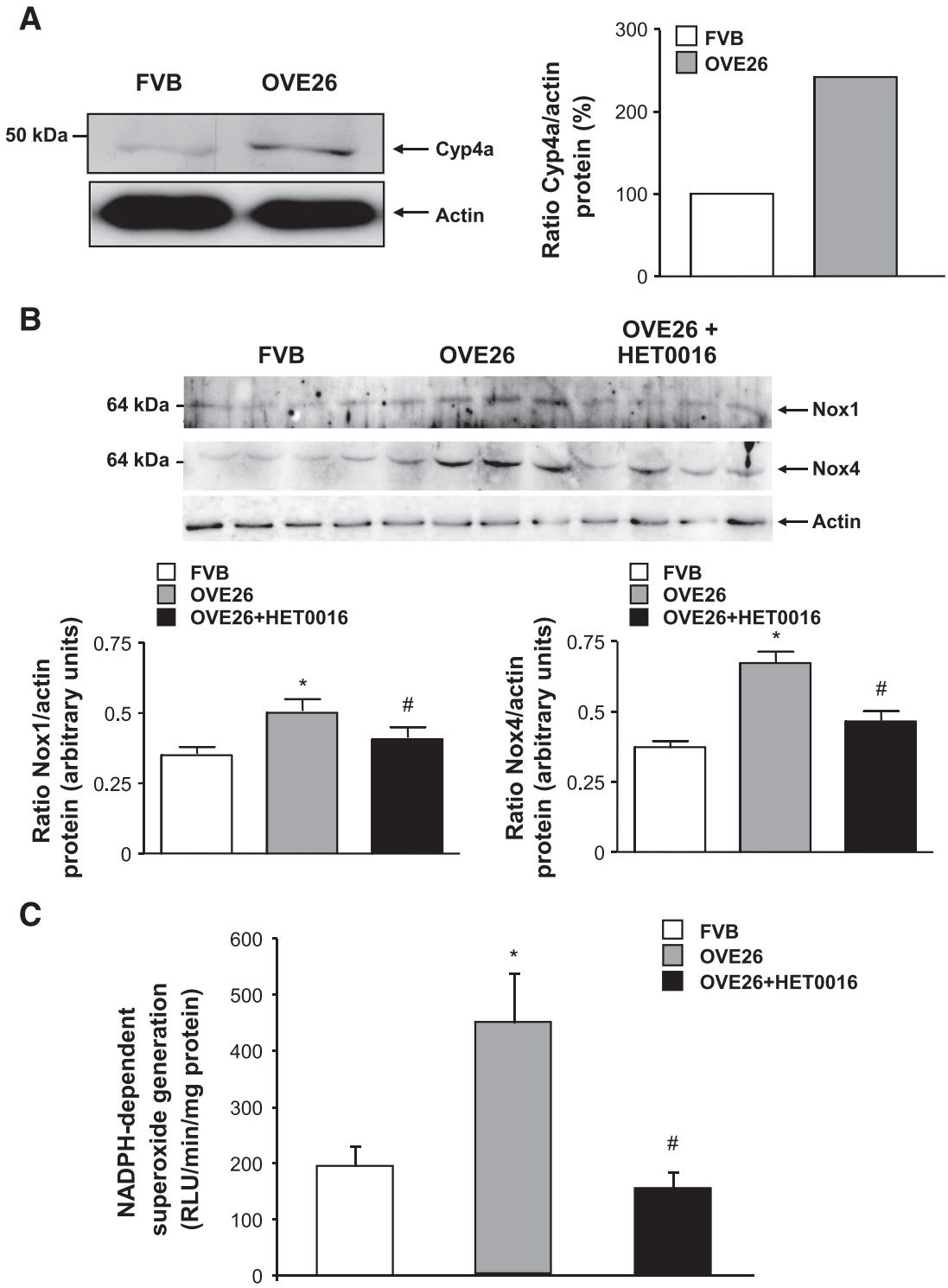

FIG. 5. CYP4A-dependent 20-HETE production contributes to Nox1 and Nox4 protein expression and NADPH oxidase activity in glomeruli of type 1 diabetic mice. *A*: Glomeruli were isolated and pooled from five separate animals. CYP4A protein expression was determined in microsomes from isolated mouse glomeruli. *B*: Glomeruli were isolated from the kidney cortex of 6-month-old OVE 26 mice, OVE 26 mice treated for 3 weeks with HET0016 (2.5 mg · kg^{-1} · day^{-1} subcutaneously), and their littermate FVB mice. Nox1 and Nox4 protein expression was determined by Western blotting. *Bottom panel*: Each histogram represents the ratio of the intensity of Nox1 or Nox4 bands factored by the actin band. Values are the means ± SE. **P* < 0.05, OVE26 mice vs. control FVB mice; #*P* < 0.05, decrease in Nox1 or Nox4 protein expression in HET0016 pretreated OVE26 mice vs. nontreated OVE 26 mice. *C*: NADPH-dependent ROS generation in glomerular homogenates isolated from the kidney cortex of FVB, OVE26, and OVE26 mice treated with HET0016 was measured by lucigenin-enhanced chemiluminescence. Superoxide anion is expressed as relative chemiluminescent light units (RLU) per milligram of protein per minute. Values are the means ± SE. **P* < 0.05, OVE26 mice vs. control FVB mice; #*P* < 0.05, decrease in NADPH oxidase activity in HET0016 pretreated OVE26 mice vs. nontreated OVE 26 mice.

albumin excretion and podocyte foot process effacement and depletion in OVE26 mice, a well-established model of type 1 diabetes.

There is good evidence that hyperglycemia and glucotoxicity contribute to podocyte injury (7). Diabetes induces oxidative stress, and podocytes are known to be

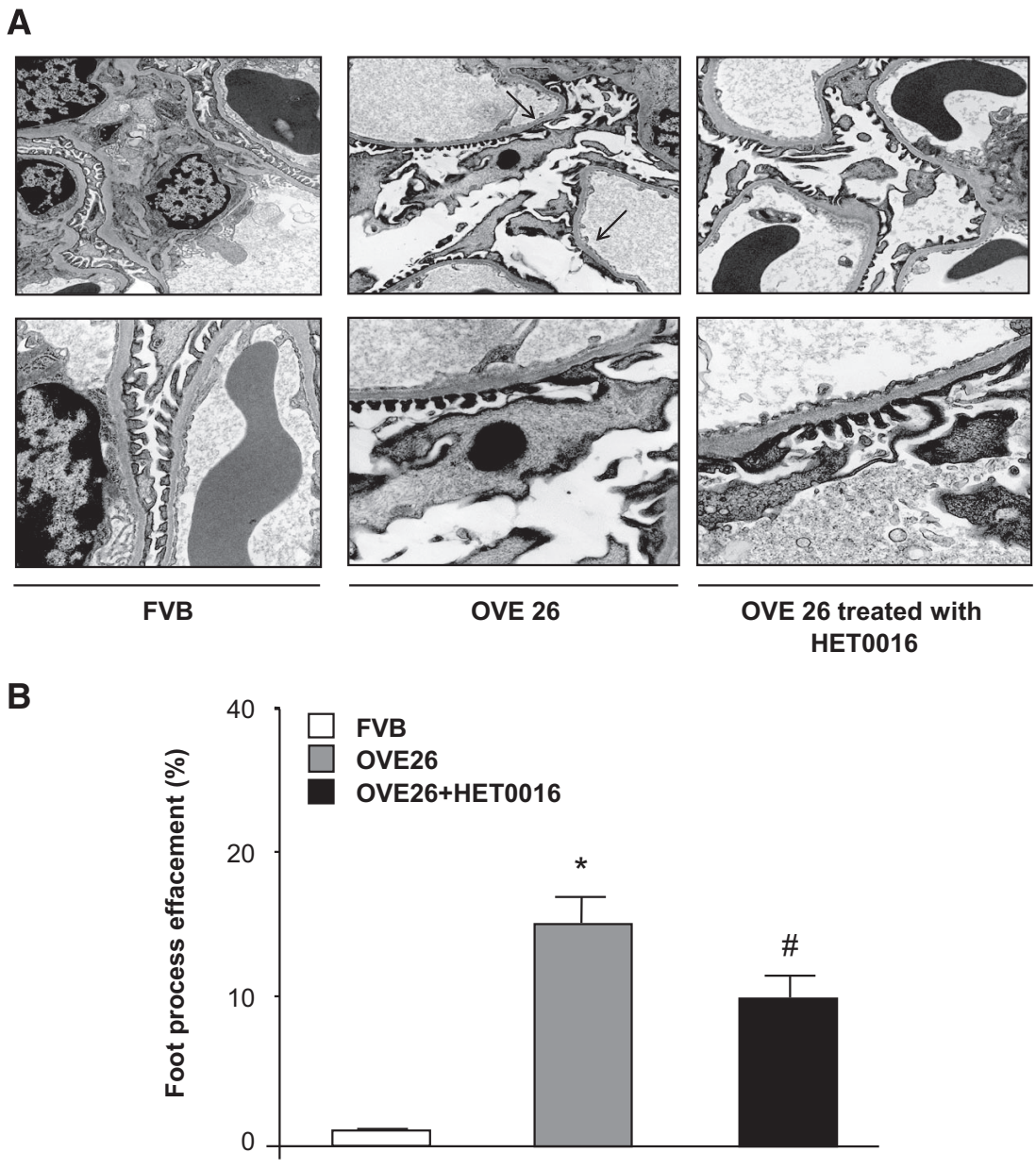

FIG. 6. CYP4A contributes to podocyte apoptosis and foot process effacement in glomeruli of type 1 diabetic mice. *A*: Representative transmission electron micrographs of glomerular cross-section of FVB, OVE26, and OVE 26 mice treated with HET0016. The images show a condensed podocyte nucleus, foot process effacement, cytoplasmic rarefication, and basement membrane thickening of an OVE26 diabetic mouse. This effect was not seen in the OVE26 mice treated with HET0016. *B*: Semiquantitative analysis of foot process effacement of glomeruli from each group of animals ($n = 5$ per group). *$P < 0.05$, OVE26 mice vs. control FVB mice; #$P < 0.05$, decrease in the percentage of foot process effacement in OVE26 mice treated with HET0016 compared with OVE26 mice.

particularly susceptible to oxidative injury (36,37). Previous studies demonstrated that intracellular ROS mediate apoptosis of podocytes in response to ANGII or high glucose (7,38). Susztak et al. (7) demonstrated that the apoptotic effect of glucose was inhibited by the superoxide dismutase mimetic tempol and inhibitors of mitochondrial respiratory chain and NADPH oxidases. However, the precise sources of ROS and the kinetics of the increase in NADPH-dependent superoxide generation have not yet been examined.

The kidney is known to express NADPH oxidase isoforms of the Nox family (13,15,35). At least three different Nox isoforms are expressed in the kidney cortex: Nox1, Nox2, and Nox4 (16). In many cells, glucose or ANGII elicit a rapid (within minutes) increase in ROS generation (7,15). We also found that high glucose rapidly increased ROS generation in cultured podocytes. However, there were no changes in NADPH oxidase activity or expression of Nox enzymes on short exposure of the cells to high glucose. This suggests that other sources of ROS may be responsible for ROS production at early time points after exposure of the cells to high glucose. There are multiple other sources of ROS in cells and tissues. ROS generation occurs as a byproduct of CYP450 enzyme activation. Mitochondria and peroxisomes are also important sources of ROS (16). CYP4A mRNA and protein are expressed in glomeruli of mice (20,25). The regulation of CYP4A and 20-HETE production is tissue- and disease specific (19). In this study, we show that CYP4A protein expression and 20-HETE production were increased within hours of expo-

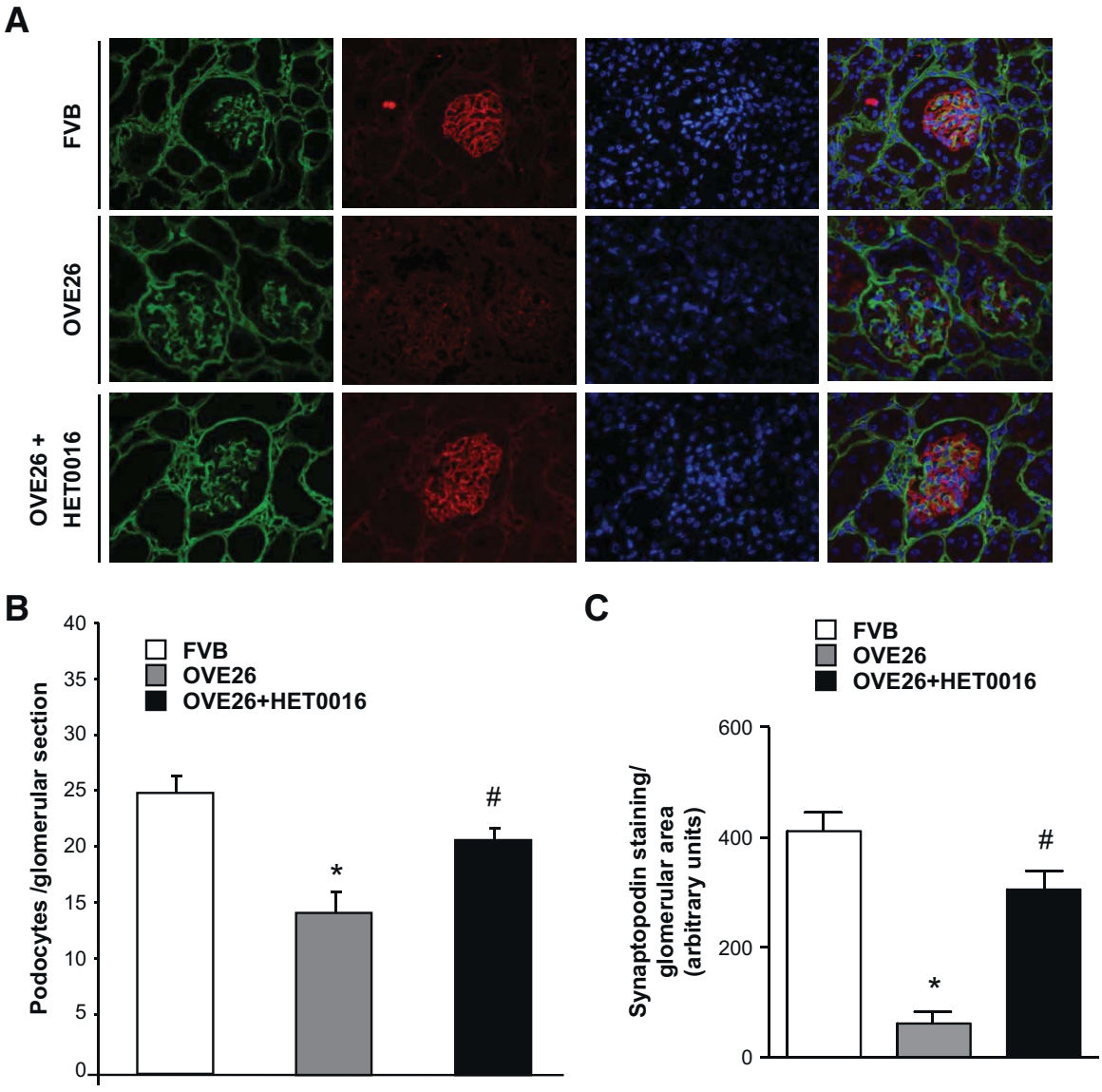

FIG. 7. CYP4A contributes to podocyte apoptosis and reduction in synaptopodin protein expression in glomeruli of type 1 diabetic mice *A*: Representative immunofluorescence images of glomeruli stained with collagen IV (green), synaptopodin (red), and 4′,6-diamidino-2-phenylindole (blue). *B*: Podocyte number per glomerular section was lower in OVE26 mice, with a significant increase in podocyte number in the OVE26 mice treated with HET0016 ($n = 5$ per group). *C*: Synaptopodin protein expression in OVE 26 mice was decreased in the OVE26 mice and restored with the injection of HET0016. Values are the means ± SE. *$P < 0.05$, OVE26 mice vs. control FVB mice; #$P < 0.05$, decrease in albumin levels in HET0016-pretreated OVE26 mice vs. nontreated OVE 26 mice ($n = 5$ per group). (A high-quality digital representation of this figure can be found in the online issue.)

sure of the cells to high glucose, at time points where no changes in NADPH oxidase activity or Nox protein expression were observed. Importantly, we show that ROS production, Nox oxidases, and apoptosis in response to glucose were inhibited when the cells were treated with HET0016, a highly specific CYP4A inhibitor. Moreover, addition of exogenous 20-HETE enhanced ROS generation and induced podocyte apoptosis. Collectively, these data indicate that CYP4A and 20-HETE generation induced podocyte apoptosis, and this biological effect was likely mediated by enhanced ROS production. There is evidence that 20-HETE mediates cytotoxicity and apoptosis in ischemic kidney tubular epithelial cells (27,39). Baliga et al. (39) also showed that inhibition of CYP450 reduced cell death in LLC-PK1 cells treated with hydrogen peroxide. It has been proposed that 20-HETE exerts its deleterious effect through the generation of ROS. Nilakantam et al. (27) showed that CYP4A12 overexpression significantly exacerbates the tubular epithelial injury that is associated with renal ischemia/reperfusion injury and that the programmed cell death is partially dependent on enhanced generation of free radicals by CYP4A. On the other hand, 20-HETE appears to play a protective role in pulmonary artery smooth muscle cells by inhibiting apoptosis (28).

To explore the relevance to type 1 diabetes of our observations in cultured podocytes, we studied an established mouse model of type 1 diabetes, the OVE 26 mouse. These mice develop morphologic and structural changes characteristic of human diabetic nephropathy (40,41). We also demonstrate that OVE26 mice exhibited thickening of the glomerular basement membrane, foot process effacement, podocyte apoptosis as seen by EM, and podocyte loss. Urinary albumin excretion in these mice was also much higher than that seen in the FVB control mice. We

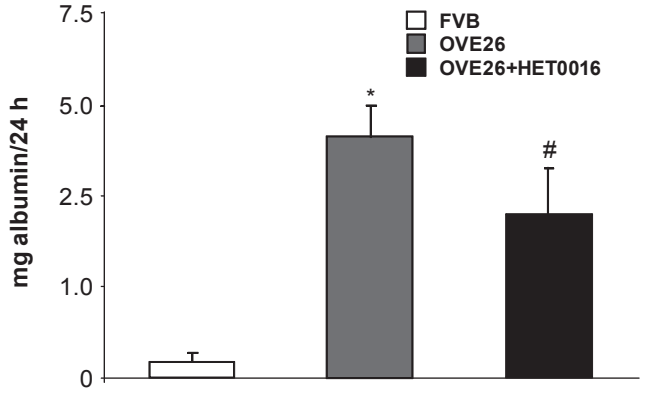

FIG. 8. CYP4A contributes to albuminuria in type 1 diabetic mice. FVB, OVE26, and OVE 26 mice treated with HET0016 were placed in metabolic cages for 24 h. Urine was collected and albumin levels were measured and expressed as milligrams of albumin per 24 h. Values are the means ± SE. *$P < 0.05$, OVE26 mice vs. control FVB mice; #$P < 0.05$, decrease in albumin levels in HET0016-pretreated OVE26 mice vs. nontreated OVE 26 mice ($n = 5$ per group).

found an increase in the expression of CYP4A protein in microsomes isolated from glomeruli of OVE 26 mice compared with glomeruli isolated from control FVB mice. Administration of a specific inhibitor of 20-HETE production, HET0016, to OVE26 mice attenuated albuminuria and reduced foot process effacement, apoptosis, and podocyte loss. Inhibition of CYP4A also resulted in downregulation of Nox1 and Nox4 protein and mRNA expression and markedly inhibited NADPH oxidase activity. These data indicate that 20-HETE plays an important role in the structural and functional changes of podocytes in type 1 diabetes. Whether the decreased expression of Nox1 or Nox4 contributes to the protective effect of CYP4A inhibition remains speculative. We recently demonstrated that NADPH-dependent ROS generation was increased in glomeruli of rats with streptozotocin-induced diabetes (13). Inhibition of Nox4 oxidase using antisense oligonucleotide therapy reduces glomerular ROS generation, glomerular hypertrophy, and fibronectin expression 2 weeks after the induction of type 1 diabetes (13). Urinary protein and albumin excretion were not measured in these studies. Sharma et al. (42) recently demonstrated that mouse podocytes expressed Nox4 and that adiponectin, which decreased podocyte permeability to albumin in vitro, reduced Nox4 expression. Therefore, the role of Nox proteins in mediating the effect of 20-HETE remains to be explored.

In conclusion, in the current study, we identified the sequential upregulation of CYP4A, 20-HETE, and Nox enzymes as sources of ROS generation that lead to apoptosis of cultured podocytes exposed to high glucose. We show that this redox pathway plays a key role in podocyte depletion and proteinuria in type 1 diabetes. These results suggest that enhanced release of 20-HETE in the diabetic state contributes to podocyte injury and that inhibitors of the CYP4A family may be therapeutically useful in the treatment of diabetic nephropathy.

ACKNOWLEDGMENTS

Support for these studies was provided by the following sources: a National Kidney Foundation Postdoctoral Fellowship (to A.A.E.), an American Heart Association South Central Affiliate and Juvenile Diabetes Research Foundation regular research grant (to Y.G.), National Institutes of Health Grant K01DK-076923 (to K.B.), National Institutes of Health, George O'Brien Kidney Center-morphology core grant no. DK061597 (to J.L.B.), and National Institutes of Health Grant DK-R01-078971 and grants from the American Diabetes Association and the Juvenile Diabetes Research Foundation (to H.E.A.).

No potential conflicts of interest relevant to this article were reported.

We thank Dr. Linda Roman for her help in measuring 20-HETE production and Sergio Garcia and Freydine Springer for technical assistance.

REFERENCES

1. De Zeeuw D, Remuzzi G, Parving H, Keane W, Zhang Z, Shahinfar S, Snapinn S, Cooper M, Mitch W, Brenner B. Proteinuria, a target for renoprotection in patients with type 2 diabetic nephropathy: lessons from RENAAL. Kidney Int 2004;65:2309–2320
2. Drummond K, Mauer M; International Diabetic Nephropathy Study Group. The early natural history of nephropathy in type 1 diabetes. II. Early renal structural changes in type 1 diabetes. Diabetes 2002;51:1580–1587
3. Pagtalunan ME, Miller PL, Jumping-Eagle S, Nelson RG, Myers BD, Rennke HG, Coplon NS, Sun L, Meyer TW. Podocyte loss and progressive glomerular injury in type II diabetes. J Clin Invest 1997;99:342–348
4. Meyer TW, Bennett PH, Nelson RG. Podocyte number predicts long-term urinary albumin excretion in Pima Indians with type II diabetes and microalbuminuria. Diabetologia 1999;42:1341–1344
5. Wolf G, Chen S, Ziyadeh FN. From the periphery of the glomerular capillary wall toward the center of disease: podocyte injury comes of age in diabetic nephropathy. Diabetes 2005;54:1626–1634
6. Steffes MW, Schmidt D, McCrery R, Basgen JM. Glomerular cell number in normal subjects and in type 1 diabetic patients. Kidney Int 2001;59:2104–2113
7. Susztak k, Raff AC, Schiffer M, Böttinger EP. Glucose-induced reactive oxygen species cause apoptosis of podocytes and podocyte depletion at the onset of diabetic nephropathy. Diabetes 2006;55:225–233
8. Kanwar YS, Liu ZZ, Kumar A, Usman MI, Wada J, Wallner EI. D-glucose-induced dysmorphogenesis of embryonic kidney. J Clin Invest 1996;98:2478–2488
9. Schiffer M, Bitzer M, Roberts IS, Kopp JB, ten Dijke P, Mundel P, Böttinger EP. Apoptosis in podocytes induced by TGF-beta and Smad7. Clin Invest 2001;108:807–816
10. Wada T, Pippin JW, Terada Y, Shankland SJ. The cyclin-dependent kinase inhibitor p21 is required for TGF-beta1-induced podocyte apoptosis. Kidney Int 2005;68:1618–1629
11. Shankland SJ, Floege J, Thomas SE, Nangaku M, Hugo C, Pippin J, Henne K, Hockenberry DM, Johnson RJ, Couser WG. Cyclin kinase inhibitors are increased during experimental membranous nephropathy: potential role in limiting glomerular epithelial cell proliferation in vivo. Kidney Int 1997;52:404–413
12. Ding G, Reddy K, Kapasi AA, Franki N, Gibbons N, Kasinath BS, Singhal PC. Angiotensin II induces apoptosis in rat glomerular epithelial cells. Am J Physiol Renal Physiol 2002;283:F173–F180
13. Gorin Y, Block K, Hernandez J, Bhandari B, Wagner B, Barnes JL, Abboud HE. Nox4 NAD(P)H oxidase mediates hypertrophy and fibronectin expression in the diabetic kidney. J Biol Chem 2005;280:39616–39626
14. Satoh M, Fujimoto S, Haruna Y, Arakawa S, Horike H, Komai N, Sasaki T, Tsujioka K, Makino H, Kashihara N. NAD(P)H oxidase and uncoupled nitric oxide synthase are major sources of glomerular superoxide in rats with experimental diabetic nephropathy. Am J Physiol Renal Physiol 2005;288:F1144–F1152
15. Kim NH, Rincon-Choles H, Bhandari B, Choudhury GG, Abboud HE, Gorin Y. Redox dependence of glomerular epithelial cell hypertrophy in response to glucose. Am J Physiol Renal Physiol 2006;290:F741–F751
16. Bedard K, Krause KH. The NOX family of ROS-generating NADPH oxidases: physiology and pathophysiology. Physiol Rev 2007;87:245–313
17. Puntarulo S, Cederbaum AI. Production of reactive oxygen species by microsomes enriched in specific human cytochrome P450 enzymes. Free Radic Biol Med 1998;24:1324–1330
18. Fleming I, Michaelis UR, Bredenkotter D, Fisslthaler B, Dehghani F, Brandes RP, Busse R. Endothelium-derived hyperpolarizing factor synthase (cytochrome P450 2C9) is a functionally significant source of reactive oxygen species in coronary arteries. Circ Res 2001;88:44–51
19. Natarajan R, Amarender Reddy M. HETEs/EETs in renal glomerular and epithelial cell function. Curr Opin Pharmacol 2003;3:198–203

20. Stec DE, Flasch A, Roman RJ, White JA. Distribution of cytochrome P-450 4A and 4F isoforms along the nephron in mice. Am J Physiol Renal Physiol 2003;284:F95–F102
21. Schwartzman ML, da Silva JL, Lin F, Nishimura M, Abraham NG. Cytochrome P450 4A expression and arachidonic acid omega-hydroxylation in the kidney of the spontaneously hypertensive rat. Nephron 1996;73:652–653
22. Dey A, Maric C, Kaesemeyer WH, Zaharis CZ, Stewart J, Pollock JS, Imig JD. Rofecoxib decreases renal injury in obese Zucker rats. Clin Sci 2004;107:561–570
23. Shimojo N, Ishizaki T, Imaoka S, Funae Y, Fujii S, Okuda K. Changes in amounts of cytochrome P450 isozymes and levels of catalytic activities in hepatic and renal microsomes of rats with streptozocin-induced diabetes. Biochem Pharmacol 1993;46:621–627
24. Sarkis A, Ito O, Mori T, Kohzuki M, Ito S, Verbalis J, Cowley AW Jr, Roman RJ. Cytochrome P-450-dependent metabolism of arachidonic acid in the kidney of rats with diabetes insipidus. Am J Physiol Renal Physiol 2005;289:F1333–F1340
25. Roman RJ, Maier KG, Sun CW, Harder DR, Alonso-Galicia M. Renal and cardiovascular actions of 20-hydroxyeicosatetraenoic acid and epoxyeicosatrienoic acids. Clin Exp Pharmacol Physiol 2000;27:855–865
26. Abboud HE, Ou SL, Velosa JA, Shah SV, Dousa TP. Dynamics of renal histamine in normal rat kidney and in nephrosis induced by aminonucleoside of puromycin. J Clin Invest 1982;69:327–336
27. Nilakantan V, Maenpaa C, Jia G, Roman RJ, Park F. 20-HETE-mediated cytotoxicity and apoptosis in ischemic kidney epithelial cells. Am J Physiol Renal Physiol 2008;294:F562–F570
28. Wang Z, Tang X, Li Y, Leu C, Guo L, Zheng X, Zhu D. 20-Hydroxyeicosatetraenoic acid inhibits the apoptotic responses in pulmonary artery smooth muscle cells. Eur J Pharmacol 2008;588:9–17
29. Jo YI, Cheng H, Wang S, Moeckel GW, Harris RC. Puromycin induces reversible proteinuric injury in transgenic mice expressing cyclooxygenase-2 in podocytes. Nephron Exp Nephrol 2007;107:e87–e94
30. Faulkner JL, Szcykalski LM, Springer F, Barnes JL. Origin of interstitial fibroblasts in an accelerated model of angiotensin II (Ang II)-induced renal fibrosis. Am J Pathol 2005;167:1193–1205
31. Kim YH, Goyal M, Kurnit D, Wharram B, Wiggins J, Holzman L, Kershaw D, Wiggins RC. Podocyte depletion and glomerulosclerosis have a direct relationship in the PAN-treated rat. Kidney Int 2001;60:957–968
32. Sanden SK, Wiggins J, Goyal M, Riggs LK, Wiggins RC. Evaluation of a thick and thin section method for estimation of podocyte number, glomerular volume, and glomerular volume per podocyte in rat kidney with Wilms' tumor-1 protein used as a podocyte nuclear marker. J Am Soc Nephrol 2003;14:2484–2493
33.. Siu B, Saha J, Smoyer WE, Sullivan KA, Brosius FC 3rd. Reduction in podocyte density as a pathologic feature in early diabetic nephropathy in rodents: prevention by lipoic acid treatment. BMC Nephrol 2006;7:6
34. Miyata N, Taniguchi K, Seki T, Ishimoto T, Sato-Watanabe M, Yasuda Y, Doi M, Kametani S, Tomishima Y, Ueki T, Sato M, Kameo K. HET0016, a potent and selective inhibitor of 20-HETE synthesizing enzyme. Br J Pharmacol 2001;133:325–329
35. Li JM, Shah AM. ROS generation by nonphagocytic NADPH oxidase: potential relevance in diabetic nephropathy. J Am Soc Nephrol 2003;14(Suppl 3):S221–S226
36. Binder CJ, Weiher H, Exner M, Kerjaschki D. Glomerular overproduction of oxygen radicals in Mpv17 gene-inactivated mice causes podocyte foot process flattening and proteinuria: a model of steroid-resistant nephrosis sensitive to radical scavenger therapy. Am J Pathol 1999;154:1067–1075
37. Greiber S, Münzel T, Kästner S, Müller B, Schollmeyer P, Pavenstädt H. NAD(P)H oxidase activity in cultured human podocytes: effects of adenosine triphosphate. Kidney Int 1998;53:654–663
38. Kang BP, Frencher S, Reddy V, Kessler A, Malhorta A, Meggs LG. High glucose promotes mesangial cell apoptosis by oxidant-dependent mechanism. Am J Physiol Renal Physiol 2003;284:F455–F466
39. Baliga R, Zhang Z, Shah SV. Role of cytochrome P-450 in hydrogen peroxide-induced cytotoxicity to LLC-PK1 cells. Kidney Int 1996;50:1118–1124
40. Epstein PN, Overbeek PA, Means AR. Calmodulin-induced early-onset diabetes in transgenic mice. Cell 1989;58:1067–1073
41. Zheng S, Noonan WT, Metreveli NS, Coventry S, Kralik PM, Carlson EC, Epstein PN. Development of late-stage diabetic nephropathy in OVE26 diabetic mice. Diabetes 2004;53:3248–3257
42. Sharma K, Ramachandrarao S, Qiu G, Usui HK, Zhu Y, Dunn SR, Ouedraogo R, Hough K, McCue P, Chan L, Falkner B, Goldstein BJ. Adiponectin regulates albuminuria and podocyte function in mice. J Clin Invest 2008;118:1645–1656